Uniaxial strain dependence of the critical current of DI-BSCCO tapes

2014 Supercond. Sci. Technol. 27 085005

(http://iopscience.iop.org/0953-2048/27/8/085005)

IOP Publishing Superconductor Science and Technology

Supercond. Sci. Technol. **27** (2014) 085005 (11pp) doi:10.1088/0953-2048/27/8/085005

Uniaxial strain dependence of the critical current of DI-BSCCO tapes

Kozo Osamura[1], Shutaro Machiya[2], Damian P Hampshire[3], Yoshinori Tsuchiya[4], Takahisa Shobu[5], Kentaro Kajiwara[6], Goro Osabe[7], Kouhei Yamazaki[7], Yuichi Yamada[7] and Jun Fujikami[7]

[1] RIAS, Kyoto 606-8202, Japan
[2] Daido University, Nagoya 457-8530, Japan
[3] University of Durham, Durham DH1 3LE, UK
[4] AIST, Tsukuba 305-8568, Japan
[5] JAEA, Tokai 319-1195, Japan
[6] JASRI, Hyogo 679-5198, Japan
[7] Sumitomo Electric Industries, Ltd, Osaka 554-0024, Japan

E-mail: kozo_osamura@rias.or.jp

Received 26 November 2013, revised 14 May 2014
Accepted for publication 21 May 2014
Published 25 June 2014

Abstract

In order to explain the effect of uniaxial strain on the critical current of DI-BSCCO-Bi2223 tapes, we employed a springboard sample holder that can smoothly and continuously apply both tensile and compressive strains to tape samples. Over a narrow tensile strain region, the critical current in the tapes decreased linearly with increasing strain and returned reversibly with decreasing strain. When compressive strain was applied, the critical current first increased and then reached a weak maximum. Thereafter, it decreased monotonically with further increases in compressive strain. At room temperature, the local strain exerted on BSCCO filaments was measured by means of a quantum beam diffraction technique. Over the whole tensile strain region up to 0.2% and the small compressive strain range, the local strain changed linearly with applied strain. When the compressive strain was applied beyond the relaxation strain, the local strain (measured by diffraction) versus the applied strain (measured using a strain gauge) deviated from linearity, which is characteristic of strain relaxation and the onset of BSCCO filament fracture. Thus, the strain at the maximum critical current corresponds to a crossover point in strain, above which the critical current decreased linearly and reversibly with increasing applied strain, and below which the critical current decreased due to the BSCCO filament fracture. In this paper, we clearly characterize the reversible range terminated by both compressive and tensile strains, in which filaments do not fracture. Our analysis of the compressive regime beyond the relaxation strain suggests that although BSCCO filament fracture is the primary factor that leads to a decrease in critical current, the critical current in those regions of filaments that are not fractured increases linearly and reversibly with decreasing applied strain at compressive strains well beyond the reversible region for the tape.

Keywords: critical current, uniaxial strain, local strain, quantum beam, BSCCO

(Some figures may appear in colour only in the online journal)

List of symbols

A_a	Applied strain
A_{acr}	Compressive relaxation strain
A_{aff}	Force free strain
A_{atr}	Tensile relaxation strain
A_i	Intrinsic strain ($A_\mathrm{i} = A\mathrm{a} - A\mathrm{p}$)

A_p	Strain at critical current maximum
$A^{lat}_{BSCCO}(A_a)$	Lattice strain exerted on BSCCO filaments
$A^{loc}_{BSCCO}(A_a)$	Local strain exerted on BSCCO filaments
A^{T}_{BSCCO}	Thermal strain exerted on BSCCO filaments
B_{c2}	Upper critical field
d^{p}_{BSCCO}	Crystal plane spacing of the BSCCO powder
$d(0)$	Crystal plane spacing at zero applied strain
$d(A_a)$	Crystal plane spacing at A_a
I_c	Critical current
I_{co}	Initial critical current at zero applied strain
$I_C(A_a = 0)$	Critical current at zero applied strain
l	Length of the tape
s	Cross sectional area of the tape
t	Thickness of the tape
T_c	Critical temperature
w	Width of the tape
α_i	Coefficient of thermal expansion of the component i
ν_i	Poisson ratio of the component i
ΔA_c	Difference between A_{acr} and A_{aff}
ΔA_t	Difference between A_{aff} and A_{atr}

1. Introduction

Practical superconducting (SC) wires are composites that only meet the desired engineering characteristics through the expert selection of materials and imaginative design of the architecture. Because of the differences in the coefficient of thermal expansion (CTE) and the modulus of elasticity between the constituent components, the macroscopic mechanical properties of composites are complicated and make it difficult to determine the local strains exerted on the SC components that influence their electromagnetic properties [1–4]. Detailed analyses of the local strains and stresses that occur throughout the interior of composites have been reported for practical SC wires of BSCCO [5], REBCO [6], and Nb_3Sn [7, 8].

The prominent feature of practical SC wires is the polycrystalline SC component. In Nb_3Sn conductors, where there is a well-established peak in the strain dependence of I_c, the strong strain dependence is attributed to the strain dependence of the SC parameters, B_{c2} and T_c, associated with the grains. This explanation has been long established from measurements on many Nb_3Sn samples in the existing literature [9]. For REBCO and BSCCO, a peak in the critical current has also been observed in the strain dependence. However, in these high temperature superconductors, the strain dependence has been attributed to changes in the properties of the grain boundaries [10–12]. Because of the prevalence of the peak in I_c versus strain in many SC wires and tapes, most papers present critical current versus strain data in terms of intrinsic strain, A_i, which is defined by: $A_i = A_a - A_p$, where A_a is the applied strain and A_p is the value of strain at which I_c reaches its peak value. In this context, it is important to know both the local strain exerted on the SC components themselves, which is generally different from A_a because of the composite nature of the SC wires and tapes, and the nature of the peak in I_c. It has been demonstrated that the local strain is nearly zero at A_p for Nb_3Sn [3, 13]. However, it is not zero for YBCO [14], and A_p changes depending on experimental conditions such as field and temperature.

Recently, high-performance DI-BSCCO tapes have been successfully commercialized using controlled over-pressure technology [15]. In order to use the tapes in high-magnetic-field applications, improvements in their current carrying capacity under different stress and strain conditions, as well as improved mechanical properties, are required. Tapes have been reinforced using the lamination of metallic sheets, which has very significantly improved both the strain tolerance of the critical current and the yield strength [1]. To understand these improvements properly, we need to analyze the influence of the local strain exerted on both the BSCCO filaments themselves and the macroscopic mechanical properties. The recent work that considered the role of grain boundaries in determining I_c [12] suggested that in BSCCO, the grain boundaries are highly resistive and semiconducting with relatively large-angle boundaries. In this paper, we intend to explain the uniaxial strain dependence of critical current using a springboard sample holder that can apply tensile and compressive strains to tapes. The critical current measurements were carried out at 77 K without external magnetic field. Using the same springboard, local strain measurements were made at room temperature using diffraction measurements at a synchrotron source. The correlation between the local strain exerted on BSCCO filaments, the mechanical properties, and the critical current has been investigated.

2. Experimental procedure

The DI-BSSCO tapes used here were fabricated by Sumitomo Electric Industries, Ltd. Two kinds of BSCCO tapes have been examined: an original bare tape (bare) with a thickness of 0.24 mm, and another 0.05 mm thick tape (SS50) which was laminated using stainless steel (SS) sheets on both sides. The bare tape was laminated with SS sheets using a Pb-free solder at a temperature between 480 and 520 K and under pretension of less than 40 N to produce SS50. The present BSCCO tapes can be considered typical composite multi-filamentary materials, where superconductive BSCCO filaments are embedded in a silver matrix and an outer silver alloy, and are laminated using SS sheets and solder to produce the tape.

In order to apply uniaxial tensile and compressive strain, the BSCCO tape was mounted on a springboard-shaped copper beryllium sample holder [16] as shown in figure 1. The springboard was 78 mm long and 15 mm wide. A 78 mm-long tape sample was soldered on the springboard. A strain gauge, 4 mm long and 2.7 mm wide, was attached onto the

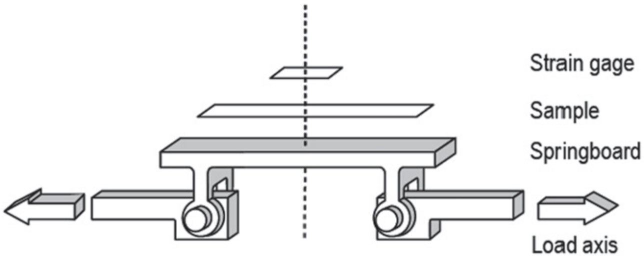

Figure 1. Springboard-shaped copper beryllium sample holder.

tape surface. The voltage taps were soldered onto the tape, 25 mm apart, outside the strain gauge. The critical current (I_c) measurement was carried out after attaching the springboard to a universal testing machine (Shimadzu AG-50kNIS). The compressive and tensile strains were applied to the tapes by pushing or pulling along the load axis and measuring the changes using the strain gauge. The critical current was determined with a criterion of 1 μV cm^{-1}. The chucking parts were electrically isolated from the tensile machine, and the sample was immersed in liquid nitrogen in an open cryostat.

The diffraction experiments were carried out at room temperature at the BL28B2 station of SPring-8. It used white x-rays with energies between 30 and 150 keV, along with the cooled Ge solid-state detector set to a diffraction angle of $2\theta = 8°$. The springboard was installed in a specially designed load frame, which was placed at the center of the goniometer. The diffraction peaks were measured while keeping the uniaxial strain constant. The diffraction geometry ensured that the scattering vector was parallel to the tape axis, and the diffraction measurements were repeated at different levels of strain. Several diffraction peaks belonging to {100} and {110} crystal planes of BSCCO were observed. In the present study, the spacing of the (220) plane was employed for local strain measurements because its diffraction intensity was strong enough to ensure sufficient statistical accuracy.

3. Experimental results

3.1. Critical current

3.1.1. Applied strain dependence of critical current. Previous studies [16, 17] have found that the critical current of BSCCO tapes decreases linearly over a small range of tensile strains, and that the critical current returns reversibly on reducing the strain. When the tensile strain increased beyond a characteristic value, the critical current decreased rapidly due to the brittle fracture of BSCCO filaments. In the present study, this behaviour was reconfirmed, as shown in figure 2.

The present critical current measurements were carried out using the following sequence of processes. During cooling, careful control of the universal testing machine ensured that no applied strain or additional external strain was applied. First, the critical current was measured at zero applied strain (I_{co}). Then, a strain was applied and I_c was remeasured. Then, the applied strain was reduced to zero and the critical current, $I_c(A_a = 0)$, was measured again. Further critical current measurements were repeated in this cyclic fashion by increasing the applied strain step by step. Figure 2 shows the results in the tensile strain region for the bare BSCCO tape.

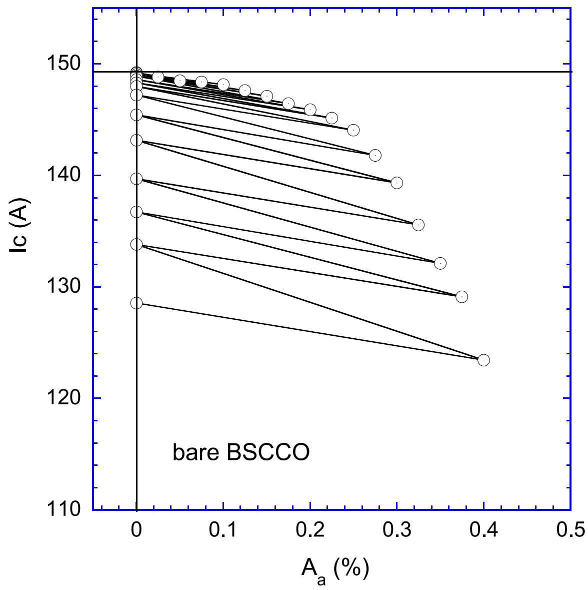

Figure 2. Critical current as a function of applied strain for the bare BSCCO tape.

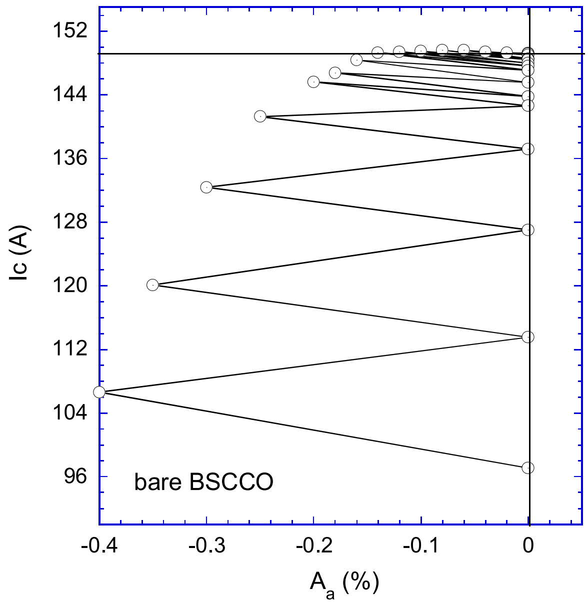

Figure 3. Critical current as a function of applied strain in the compressive strain region for the bare BSCCO tape.

The result for the compressive strain region is indicated in figure 3. When the compressive applied strain increased, the critical current increased and reached a weak maximum at about −0.08% strain. Thereafter, I_c decreased monotonically upon increasing the compressive applied strain.

Similar results for the SS50 BSCCO tape are shown in figure 4 for the tensile strain region and in figure 5 for the

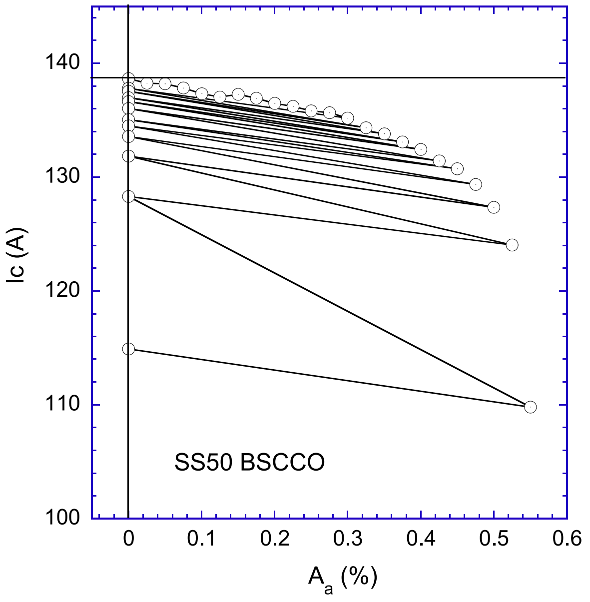

Figure 4. Critical current as a function of applied strain in the tensile strain region for the SS50 BSCCO tape.

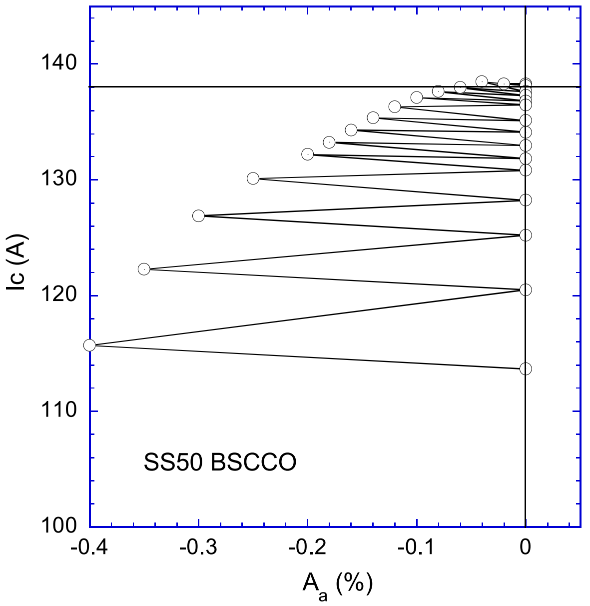

Figure 5. Critical current as a function of applied strain in the compressive strain region for the SS50 BSCCO tape.

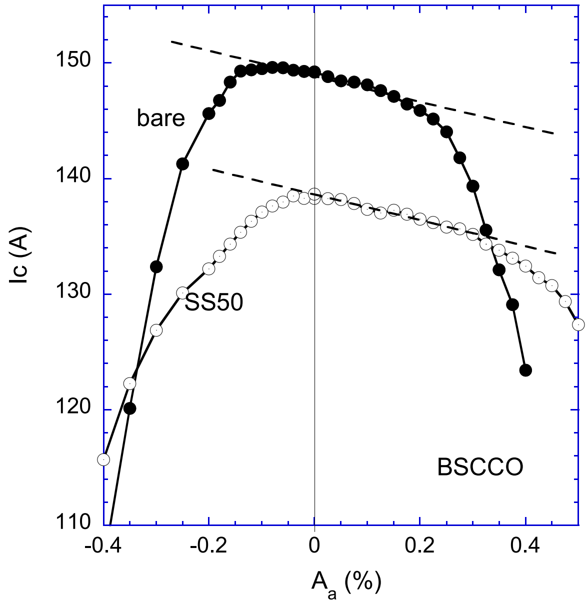

Figure 6. Applied strain dependence of the critical current for the bare and the SS50 BSCCO tapes.

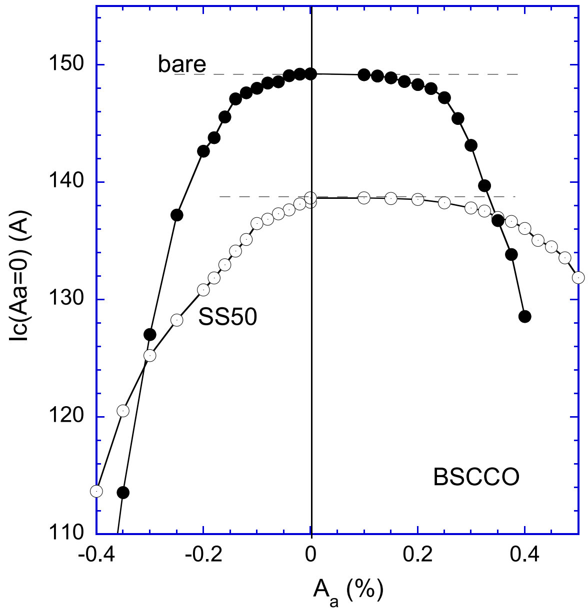

Figure 7. Applied strain dependence of $I_c(A_a = 0)$ for the bare and SS50 BSCCO tapes.

compressive strain region. A weak maximum of critical current was observed at −0.04% strain.

By extracting the data applying the strain A_a from figures 2–5, figure 6 shows the overview of the applied strain dependence of critical current for the bare and the SS50 BSCCO tapes. Over a narrow tensile strain region, the change in critical current can be expressed using the linear function proposed before, and indicated by dotted lines in figure 6 [1, 16].

$$I_c = I_{co} - kA_a \tag{1}$$

where I_{co} is the initial critical current at zero applied strain, A_a is the applied strain, and k is constant. The quotient (k/I_{co}) became the same as 0.080 [A/%] for the bare and the SS50 BSCCO tapes, while the slopes, k, for both tapes were not equal to each other as an experimental result. However, if one considers a wider range of strain, the functional form eventually becomes nonlinear.

The highlight of the present study is to clarify the appearance and role of the critical current maximum in the compressive applied strain region. Such a critical current maximum has been observed in Nb_3Sn [9] and REBCO systems [14, 18, 19]. As discussed later in this paper, we suggest that the origin of the critical current maximum is different in BSCCO than it is in REBCO and Nb_3Sn.

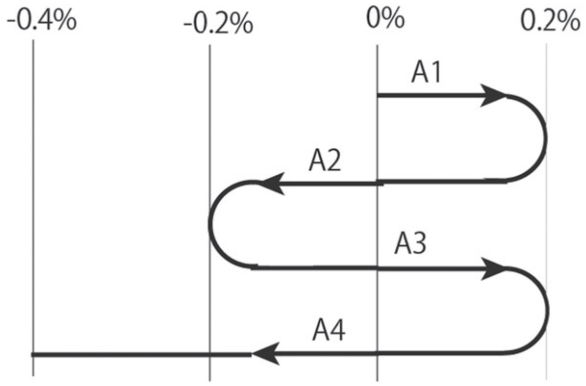

Figure 8. Illustration of the experimental sequence for applying uniaxial tensile and compressive strain by means of the springboard sample holder.

Figure 7 shows the applied strain dependence of $I_c(A_a = 0)$, which is the critical current at $A_a = 0$ (i.e., after returning back to zero applied strain) for the bare and the SS50 BSCCO tapes. The critical current data given in figure 7 indicate the recovery of the tape after applying the external strain. The recovered critical current decreases with increasing uniaxial tensile and compressive applied strain. This convex behavior is not symmetric with respect to the applied strain, and the centers of the convex curves are located at tensile strains between 0.05 and 0.1%.

3.1.2. Reversibility. To clarify the compressive strain dependence of critical current, the uniaxial strain was smoothly varied over tensile and compressive strains, as indicated in figure 8.

The results are shown in figure 9. During A1, the applied strain was increased in tension up to 0.2% and then reduced to zero. The changes in strain produced reversible changes in critical current, I_c. During A2, on increasing compression, I_c increased, reached a maximum, and then decreased. Thereafter, upon reducing the compressive strain, I_c decreased gradually. During A3, the initial strain dependence was similar to that during A1, but a hysteresis was observed. During A4, I_c increased slightly and then reached a broad maximum, beyond which it decreased greatly. These observations are similar to those reported previously [16].

3.2. Local strain exerted on BSCCO filaments

It is important to get direct information about the local strain exerted on BSCCO filaments to properly investigate its effect on critical current. The measurement of the local strain was carried out at room temperature. In order to know the strain-free state, fine BSCCO powder was extracted from the same tape sample. Such isolated homogeneous powder with a size of less than a few micrometers is expected to carry no residual strain. Hence, we use the crystal plane spacing of the powder to define the strain-free plane spacing, d^p_{BSCCO}. When the plane spacing from the tape attached to the springboard at $A_a = 0$ is

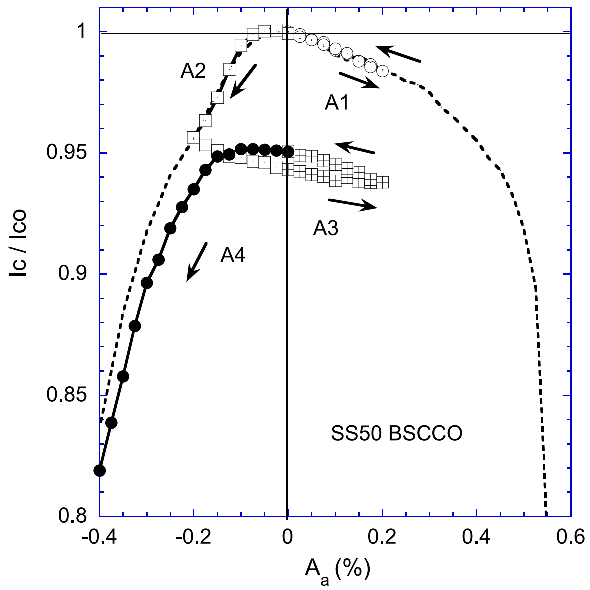

Figure 9. Change of the normalized critical current as a function of applied strain for the SS50 BSCCO tape, where the uniaxial strain was applied following the sequence shown in figure 8. The dotted curve indicates the trace of the strain dependence of critical current shown in figure 6.

$d(0)_{BSCCO}$, the *thermal strain* is given by the equation

$$A^T_{BSCCO} = \frac{\left[d(0)_{BSCCO} - d^p_{BSCCO}\right]}{d^p_{BSCCO}} 100\ [\%]. \qquad (2)$$

When external strain is applied by the springboard, BSCCO filaments elongate or shrink and the crystal plane spacing changes from $d(0)_{BSCCO}$ to $d(A_a)_{BSCCO}$. The *lattice strain* is defined as

$$A^{lat}_{BSCCO}(A_a) = \frac{d(A_a)_{BSCCO} - d(0)_{BSCCO}}{d^P_{BSCCO}} \cdot 100[\%]. \qquad (3)$$

Then, the *local strain* exerted on the BSCCO filaments becomes the sum of the lattice strain and thermal strain, given by the equation

$$A^{loc}_{BSCCO}(A_a) = A^T_{BSCCO} + A^{lat}_{BSCCO}(A_a). \qquad (4)$$

The change of local strain exerted on BSCCO filaments is shown in figure 10. At the beginning of the measurements, the thermal strain was determined as $A^T_{BSCCO} = -0.023\%$ at $A_a = 0$. During A1, as indicated in figure 8, the local strain increased linearly up to 0.2% and decreased reversibly to zero strain. The slope was estimated as

$$\frac{dA^{loc}_{BSCCO}}{dA_a} \cong 0.75, \qquad (5)$$

which is less than unity. Hence, equation (4) can be experimentally expressed as

$$A^{loc}_{BSCCO}(A_a) = -0.023 + 0.75 \cdot A_a. \qquad (6)$$

In general, because of the anisotropy of elastic constants, the slope in equation (6) determined from a specific

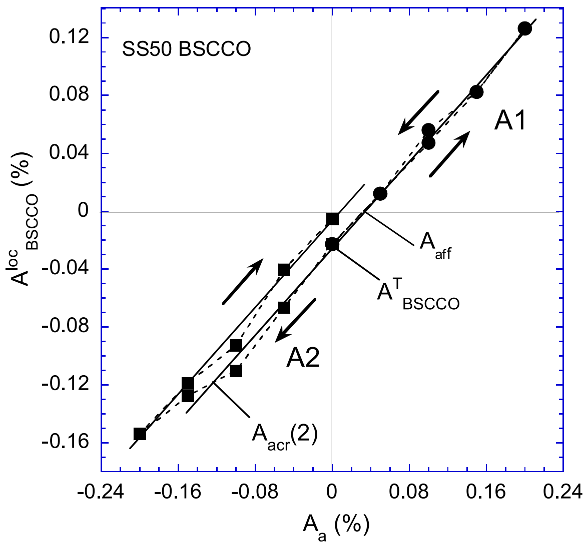

Figure 10. Change of local strain exerted on BSCCO filaments as a function of applied strain at room temperature for the SS50 BSCCO tape during A1 and A2.

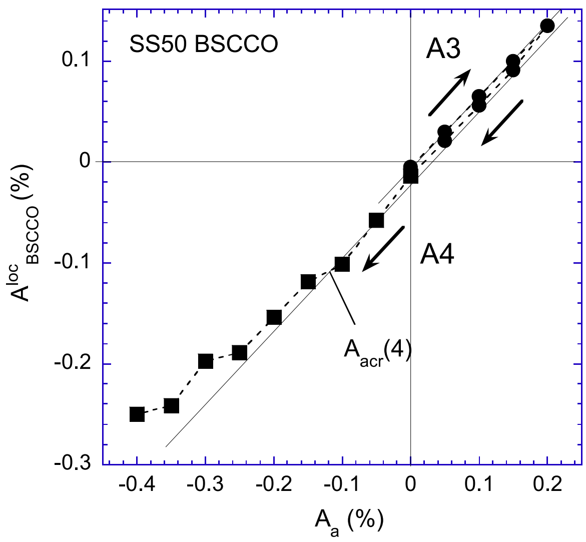

Figure 11. Change of local strain exerted on BSCCO filaments as a function of applied strain at room temperature for the SS50 BSCCO tape during A3 and A4.

diffraction peak may take a real number apart from unity, as discussed below. Figure 10 shows that the local strain exerted on BSCCO filaments became zero at a specific applied strain of $A_{aff} = 0.031\%$, which is called the force free strain [5]. During A2, the local strain decreased linearly with the same slope. Beyond a compressive strain of −0.12%, the local strain deviated upwards, which means that strain relaxation took place. When BSCCO filaments partially fracture, the elastic strain reduces, so −0.12% is the compressive relaxation strain during A2 ($A_{acr}(2)$). When reducing the compressive strain, the local strain decreased linearly with the same slope.

During the increase and decrease of strain at A3, figure 11 shows that the local strain changes were mostly linear, but include a hysteresis. During A4, the local strain

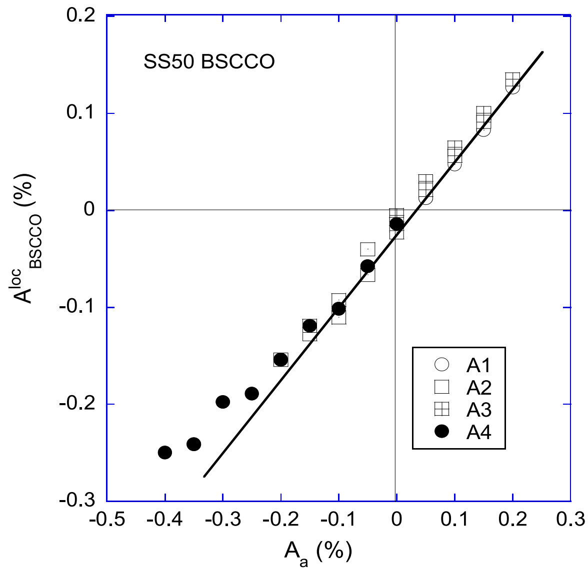

Figure 12. Overview of the applied strain dependence of local strain exerted on BSCCO filaments at room temperature for the SS50 BSCCO tape.

changes with nearly the same slope as before and deviated upwards at a relaxation strain of $A_{acr}(4) = -0.12\%$ in figure 11, which was nearly the same as $A_{acr}(2)$ in figure 10.

As shown in figure 12, the slope is constant in the reversible region of uniaxial tensile and compressive strain, as given by equation (5). The local strain deviated upwards beyond the relaxation strain, A_{acr}, at approximately −0.1%. This relaxation is attributed to the partial fracture of BSCCO filaments, as discussed in the following section.

4. Discussion

4.1. Contribution from the bending strain

When the tape sample is soldered to the springboard and bent by pushing or pulling the legs of the springboard, the strain is predominantly uniaxial, but there is also a non-negligible bending strain because of the finite thickness of the tape. A preliminary finite-element analysis shows that the bending strain was about 10 to 18% of the uniaxial strain for the current experimental conditions. However, to keep the discussion straightforward, the contribution from the bending strain component was not considered in the present study.

4.2. Slope of A^{loc}_{BSCCO} versus A_a

Equation (5) shows that the slope of A^{loc}_{BSCCO} versus A_a was less than unity. This fact is attributed to the following two reasons when the springboard is used as the present study. When uniaxial stress applies to the polycrystalline sample, individual grains deform along the force axis by an amount proportional to the elastic constant, and specific to the grain's own crystal orientation. This phenomenon has been well established in discussions of the elastic properties obtained using diffraction data [20]. A typical example appears in the REBCO coated conductors [6], in which the microtwins are distributed in the grains. Three elastically different components exist in each grain along the tape axis, that is [100] and [010] oriented crystals and twin boundaries. Their elastic constant is different from each other. As a result, the degree of deformation differs in each component and the relevant slope of A^{loc} versus A_a is not unity for all the diffraction peaks.

In the BSCCO tape, the filaments consist of small, well-oriented, plate-like crystals, where the crystal axes are mostly <100> and <110> along the tape axis. They include both small- and wide-angle grain boundaries. Consistent with a recent report [1], the slope from equation (5) derived from the spacing of the (220) plane was about 0.84 when the same BSCCO tape investigated in this paper was tested using a tensile machine, which applies an exactly uniaxial tensile stress.

As shown in figure 1, the strain gauge was attached on the tape surface. Therefore, the measured strain, A_a, was more highly estimated than the strain exerted on the BSCCO filaments because the surface of the tape is further from the neutral axis of the springboard than the filaments. In the present experiment, this overestimate is ~11.8%. Consequently, the first-order corrected slope, $0.84 \times (1 - 0.118) = 0.74$, is consistent with the diffraction data (equation (5)).

4.3. Influence of the springboard on the thermal strain

After soldering the tape sample on the springboard, cooling it down to room temperature, and then further cooling it to liquid nitrogen temperature, a thermal strain is generated in the BSCCO filaments. The volume of the springboard is so large compared with the tape that the thermal shrinkage broadly follows the thermomechanical properties of the springboard. The BSCCO filaments and springboard behave elastically in the temperature range from soldering temperature to room temperature, so, as we explain in the appendix, the thermal strain exerted on BSCCO filaments can be approximated by

$$A^T_{BSCCO} \cong (\alpha_{SB} - \alpha_{BSCCO})\Delta T, \tag{7}$$

where α_{SB} and α_{BSCCO} are the CTE of the springboard and BSCCO filaments, and ΔT is the temperature difference between the soldering temperature and room temperature. Using $\alpha_{SB} = 16.6 \cdot 10^{-6}[1/K]$, $\alpha_{BSCCO} = 15.4 \cdot 10^{-6}[1/K]$, [5] and $DT = -150\text{K}$, equation (7) gives $A^T_{BSCCO} \cong -0.018\%$. This result is consistent with the observed thermal strain of -0.023% shown in figure 10.

4.4. Relaxation strain due to the fracture of BSCCO filaments

BSCCO filaments are oxide materials that are very brittle and fracture easily. We suggest that BSCCO filaments start to fracture at the relaxation strain, A_{acr}, as shown in figure 13. The local strain exerted on BSCCO filaments becomes zero at the force free strain, A_{aff}, and the difference, $A_{acr} - A_{aff}$, corresponds to the net value of compressive fracture strain (ΔA_c), where

$$\Delta A_c = A_{acr} - A_{aff}. \tag{8}$$

Given that $A_{acr}(2) \approx A_{acr}(4) = -0.12\%$ was observed in figure 10, the net compressive fracture strain is calculated to be $DA_c = -0.15\%$. In previous research the relevant net tensile fracture strain, ΔA_t, of BSCCO filaments was reported as 0.16% [1] for the same BSCCO tape laminated by SS with a thickness of 50 μm. The solid straight line in figure 13 provides the relation given by equation (6), which holds in the elastic region between A_{acr} and A_{atr}.

4.5. Estimation of the relaxation strain at 77 K

In the present case, the thermal strain exerted on the BSCCO filaments can be evaluated from equation (7) as 0.042% at 77 K. The local strain at 77 K is then given by the equation,

$$A^{loc}_{BSCCO}(A_a) = -0.042 + 0.75 \cdot A_a. \tag{9}$$

Here, it has been assumed that the slope at 77 K is the same as equation (5) at room temperature. This assumption is reasonable since the moduli of elasticity for BSCCO and the springboard are not expected to change significantly between room temperature and 77 K. Equation (9) is shown by the dotted line in figure 13. From the crossover points, the relaxation strains at 77 K under compression and tension were obtained to be $A_{acr} = -0.07\%$ and $A_{atr} = 0.24\%$, respectively. Figure 13 emphasizes that the relationship between the applied strain and the local strain at 77 K is similar to that at room temperature. This result is assumed in the discussion in the following section.

4.6. Maximum of critical current

As shown in figure 6, there is an apparent maximum in I_c in the compressive strain region. Numerical values are listed in table 1. This work has found that BSCCO filaments fracture at the relaxation strain when the compressive applied strain increased. The relaxation strain was estimated as $A_{acr} = -0.07\%$ at 77 K. There is also some indication that the relaxation strain shifts to the less compressive strain value when the temperature decreases.

When comparing the relaxation strain with the observed value of A_{max} listed in table 1, they coincide reasonably well, so we conclude that the maximum of critical current appears at the point where the local strain changes its slope, as shown in figure 14. However, the fracture mode of BSCCO filaments has been not made clear in the present study. One can expect that the fracture under compression is more complicated than the fracture under tension. One possibility suggested by Sunwong *et al* [16], is that the strong two-dimensionality of BSCCO crystals leads to filament buckling or intragranular cracking under strain.

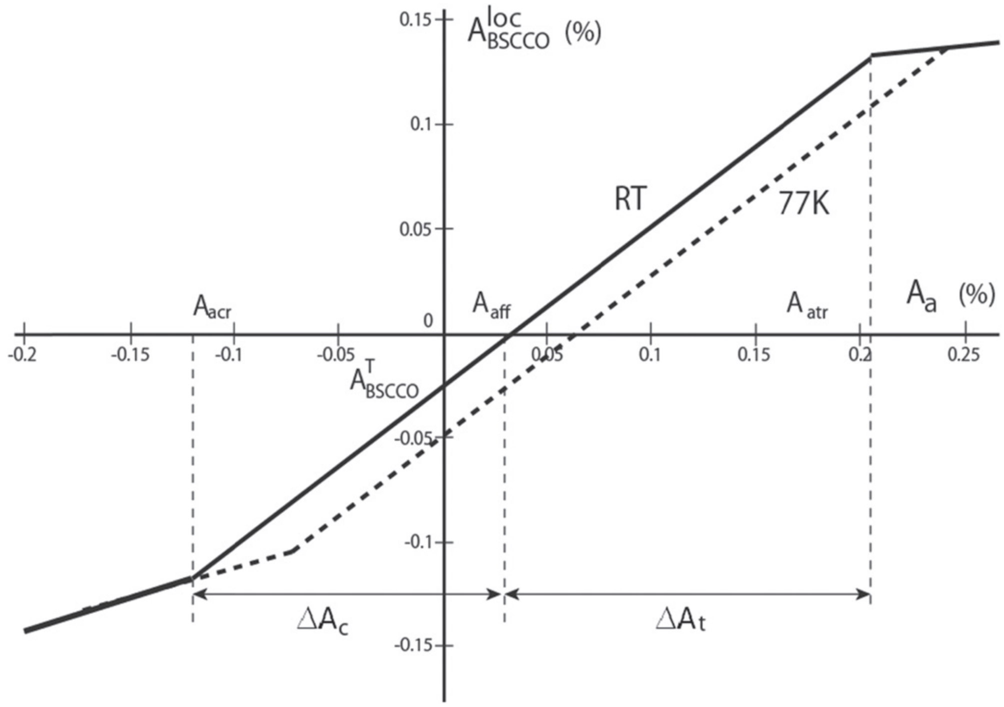

Figure 13. Applied strain dependence of the local strain exerted on BSCCO filaments at room temperature and 77 K.

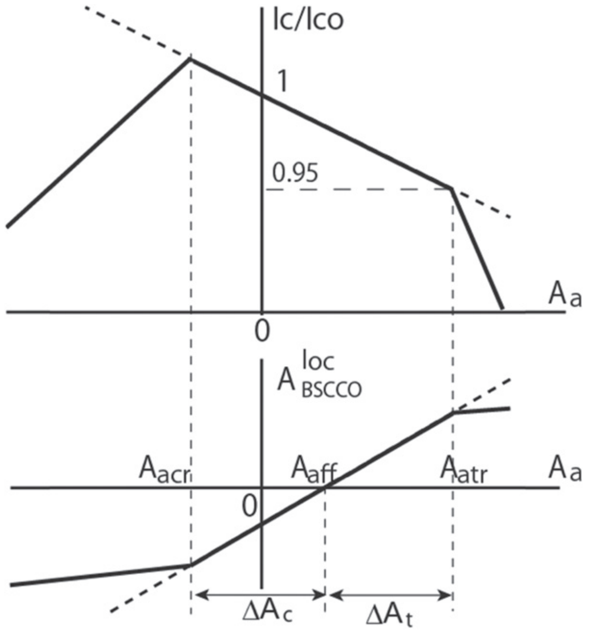

Figure 14. Schematic illustration of the reversible region, where BSCCO filaments do not fracture.

Table 1. Summary relating to the apparent maximum of critical current.

Sample	I_{co} (A)	I_{cmax}/I_{co}	A_{max} (%)
Bare	138	1.003	−0.08
SS50	149	1.002	−0.04

4.7. Applied strain dependence of the critical current for the bare BSCCO tape

As shown in figures 6 and 7, the applied strain dependence of I_c and $I_c(A_a = 0)$ for the bare BSCCO tape is very similar to the SS50 tape. This means that the local strain exerted on BSCCO filaments for the bare tape depends on the applied strain, in a similar manner for the SS50 tape, as shown in figure 13. Of course, it is not exactly the same, but qualitatively gives the same behavior. The convex strain dependency of critical currents can be explained in terms of the change of local strain, as shown in figure 14.

4.8. The reversible strain region

In order to determine the range of strain over which there is no filament fracture and the critical current is reversible, it is necessary to discuss the strain dependence of critical current and the brittle fracture of the BSCCO filaments. This work shows that the compressive relaxation strain, A_{acr}, occurs roughly when the critical current maximum is reached. As shown in figure 14, we take the tensile relaxation strain, A_{atr}, to coincide with the strain at which there is a 95% I_c retention, as reported previously [1]. The force free strain, A_{aff}, is located between the middle of the compressive and tensile relaxation strains. The compressive and tensile fracture strains, ΔA_c and ΔA_t, are as shown in figure 14. Thus, the sum $|\Delta A_c| + |\Delta A_t|$ is the width of the reversible strain region over which there is no filament fracture.

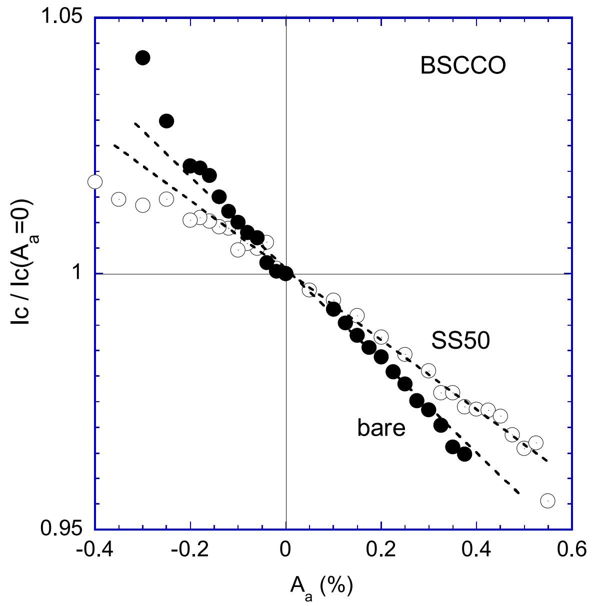

Figure 15. Strain dependence of the critical current associated with the intact regions of filaments, normalized by $I_c(A_a = 0)$ for the bare (●) and the SS50 (○) BSCCO tapes.

4.9. Strain dependence of the critical current associated with the intact regions of filaments

Figure 7 shows that the critical current at $A_a = 0$, that is $I_c(A_a = 0)$, gives a convex strain dependence. When applying excess strain, part of the filament starts to fracture. Consistent with the linearity of the diffraction data during unloading, we assume that the unfractured parts remain intact during unloading to zero applied strain, and hence identify $I_c(A_a = 0)$ as the I_c from those parts of the filament that are not fractured after unloading from A_a.

The applied strain dependence of critical current normalized by $I_c(A_a = 0)$ is shown in figure 15. The increase in $I_c/I_c(A_a = 0)$, with decreasing applied strain over the whole region of applied strain, provides evidence that the extended linear strain dependence gives the behaviour of those parts of the filaments that remain intact, after excluding the influence of BSCCO filament fracture. Hence, the intrinsic reversible strain region for BSCCO is larger than currently achieved in the tape. This linear strain dependence is qualitatively consistent, with straightforward geometrical changes in the thickness of the grain boundaries where higher supercurrents pass through thinner grain boundaries [12].

4.10. Influence of shrinkage of the cross sectional area to critical current density

The DI-BSCCO tape consists of several tens of BSCCO filaments, each of which carries supercurrent. After the deformation of the tape, we can idealize the cross section of each filament as cuboid. When a uniaxial strain is applied to the tape, each filament elongates along the applied load by $l_o A_a/100$, while it shrinks along the orthogonal directions by $\nu_t t_o A_a/100$ and $\nu_w w_o A_a/100$, where l_o, t_o, and w_o are length, thickness, and width, respectively, and ν_t and ν_w are the Poisson ratios. Then, the cross sectional area is given by the equation

$$s = s_o\left(1 - \nu_t A_a/100\right)\left(1 - \nu_w A_a/100\right). \tag{10}$$

As the critical current density, J_c, is defined by I_c/s, its derivative with applied strain is

$$\frac{\partial J_c}{\partial A_a} = \frac{1}{s}\left(\frac{\partial I_c}{\partial A_a}\right) - \frac{I_c}{s^2}\left(\frac{\partial s}{\partial A_a}\right). \tag{11}$$

The first term on the right-hand side can be rewritten using equation (1), where

$$\frac{\partial I_c}{\partial A_a} = -k_o \tag{12}$$

and k_o is a constant. In the limit of $A_a \to 0$, equation (11) is given by

$$\frac{\partial J_c}{\partial A_a} \cong \frac{I_{co}}{s_o}\left(-\frac{k_o}{I_{co}} + \frac{\nu_t + \nu_w}{100}\right). \tag{13}$$

Hence, there are two contributions to changes in I_c with applied strain: the intrinsic strain dependence of J_c and changes in filament shape associated with the Poisson ratio. The experimentally obtained quotient k/I_{co} in equation (1) measures both contributions and is simply equal to $k_o/I_{co} - (\nu_t + \nu_w)/100$. As reported previously [6, 7], the Poisson ratios for REBCO, Nb_3Al, and Nb_3Sn are observed to be in the range between 1/4 and 1/2. Recently, the elastic constants of BSCCO and YBCO crystals have been theoretically evaluated using density functional theory (DFT) by Clark [21]. In the case of YBCO, the observed Poisson ratios [6] agree with theoretical values and confirm the observed tendency for $\nu_{010} > \nu_{100}$. In the case of BSCCO, DFT suggests $\nu_t = 0.16$ and $\nu_w = 0.47$. If we make the simplifying assumption that the grain boundaries have the same Poisson ratio and local strain as the grains, we can use the theoretical values for the Poisson ratios to find $(\nu_t + \nu_w)/100 = 0.0063$. The quotient, k_o/I_{co}, is estimated to be 0.086 when $k/I_{co} = 0.080$. Hence, we conclude that the contribution from shrinkage associated with the Poisson ratios for BSCCO through the term $(\nu_t + \nu_w)/100$ is only about 8%.

5. Conclusion

The uniaxial tensile and compressive strain dependence of critical current was investigated for DI-BSCCO tapes. In the narrow tensile strain region, the critical current decreases linearly with increasing strain, and returned reversibly with decreasing strain. When compressive strain was applied, the critical current increased and reached a weak maximum. Then, it decreased monotonically by increasing the compressive applied strain.

At room temperature, the local strain exerted on BSCCO filaments was measured in the same uniaxial strain region. In the tensile strain range up to 0.2%, the local strain changed linearly with applied strain. When compressive strain was applied beyond the relaxation strain, the local strain deviated upwards, which is attributed to the partial fracture of BSCCO filaments. We suggest that the strain relaxation due to the partial fracture of BSCCO filaments takes place in a similar way at 77 K, but there is a small shift in the strain value towards the tensile strain side. The thermal strain exerted on BSCCO filaments and the force free strain, A_{aff}, were greatly influenced by the springboard because its volume fraction is so large compared to the tape, and therefore the thermal shrinkage broadly obeys the thermomechanical properties of the springboard. BSCCO filaments start to fracture at the relaxation strain, A_{acr}. The net value of compressive fracture strain was given by $\Delta A_c = A_{acr} - A_{aff}$, while the tensile fracture strain is given by $\Delta A_t = A_{atr} - A_{aff}$, where A_{atr} is the tensile relaxation strain. Thus, the sum $|\Delta A_c| + |\Delta A_t|$ is the strain width of the reversible region over which there is no filament fracture.

The compressive relaxation strain and the strain at the maximum critical current coincide reasonably well with each other, suggesting that the critical current increases with decreasing applied strain, but beyond the relaxation strain the critical current decreases due to the BSCCO filament fracture. We suggest that the critical current of those parts of the BSCCO filaments that remain intact increases linearly with decreasing applied strain over a wider uniaxial strain region than the reversible regime found for the tape.

Acknowledgements

The authors express their thanks to Professor S J Clark, University of Durham, for his valuable information. This work was supported in part by a grant-in-aid from the Ministry of Education, Culture, Sports, Science, and Technology of Japan (21360312). The synchrotron radiation experiments were performed at the BL28B2 of SPring-8 with the approval of the Japan Synchrotron Radiation Research Institute (JASRI) (proposal no. 2012B1435).

Appendix: Estimation of thermal strain exerted on BSCCO filaments

As shown in figure 1, the BSCCO tape with a thickness of 0.3 mm was soldered onto the springboard, which has a thickness of 2.5 mm. The modulus of elasticity of the whole body is given by

$$E_c = V_{fBSCCO}E_{BSCCO} + V_{fAg}\omega_{Ag}E_{Ag} + V_{fAgAlloy}E_{AgAlloy} + V_{fSolder}\omega_{Solder}E_{Solder} + V_{fSS}E_{SS} + V_{fSB}E_{SB}, \quad \text{(A1)}$$

where V_{fi}, E_i, and ω are the volume fraction, the modulus, and the work hardening coefficient of component i, respectively. Using the same procedure as that reported previously [1, 17], the thermal strain exerted on BSCCO filaments can be estimated by

$$A^T_{BSCCO} = \frac{\begin{aligned}&(\alpha_{Ag} - \alpha_{BSCCO})V_{fAg}\omega_{Ag}E_{Ag} \\ &+ (\alpha_{AgAlloy} - \alpha_{BSCCO})V_{fAgAlloy}E_{AgAlloy} \\ &+ (\alpha_{Solder} - \alpha_{BSCCO})\omega_{Solder}V_{fSolder}E_{Solder} \\ &+ (\alpha_{SS} - \alpha_{BSCCO})V_{fSS}E_{SS} \\ &+ (\alpha_{SB} - \alpha_{BSCCO})V_{fSB}E_{SB}\end{aligned}}{E_c}\Delta T, \quad \text{(A2)}$$

where $\Delta T = T_1 - T_2$ when T_1 and T_2 are the room temperature and the soldering temperature, respectively. The volume fraction of each component was estimated as $V_{fBSCCO} = 0.027$, $V_{fAg} = 0.018$, $V_{fAgAlloy} = 0.019$, $V_{fSolder} = 0.009$, $V_{fSS} = 0.035$ and $V_{fSB} = 0.892$. In the present case, the work hardening coefficient is less than 0.01 for silver and solder, so the major term that contributes to the thermal strain comes from the springboard, with successively smaller contributions coming from the Ag alloy and the SS laminated sheets. To a first approximation, accurate to about 90%, the thermal strain is given by:

$$A^T_{BSCCO} \cong (\alpha_{SB} - \alpha_{BSCCO})\Delta T. \quad \text{(A3)}$$

References

[1] Osamura K, Machiya S, Ochiai S, Osabe G, Yamazaki K and Fujikami J 2013 Direct evidence of the high strain tolerance of the critical current of DI-BSCCO tapes fabricated by means of the pretensioned lamination technique *Supercond. Sci. Technol.* **26** 045012

[2] Osamura K, Machiya S, Tsuchiya Y and Suzuki H 2010 Force free strain exerted on a YBCO layer at 77 K in surround Cu stabilized YBCO coated conductors *Supercond. Sci. Technol.* **23** 045020

[3] Osamura K, Machiya S, Tsuchiya Y, Suzuki H, Shobu T, Sato M, Hemmi T, Nunoya Y and Ochiai S 2012 Local strain and its influence on mechanical-electromagnetic properties of twisted and untwisted ITER Nb3Sn strands *Supercond. Sci. Technol.* **25** 054010

[4] Osamura K, Machiya S, Ochiai S, Osabe G, Yamazaki K and Fujikami J 2013 High strength/high strain tolerance DI-BSCCO tapes by means of pre-tensioned lamination technique *IEEE Trans. Appl. Supercond.* **23** 6400504

[5] Osamura K, Machiya S, Suzuki H, Ochiai S, Adachi H, Ayai N, Hayashi K and Sato K 2008 Mechanical behavior and strain dependence of the critical current of DI-BSCCO tapes *Supercond. Sci. Technol.* **21** 054010

[6] Osamura K, Machiya S, Tsuchiya Y, Suzuki H, Shobu T, Sato M and Ochiai S 2012 Microtwin structure and its influence on the mechanical properties of REBCO coated conductors *IEEE Trans. Appl. Supercond.* **22** 8400809

[7] Osamura K *et al* 2013 Thermal strain exerted on superconductive filaments in practical Nb_3Sn and Nb_3Al strands *Supercond. Sci. Technol.* **26** 094001

[8] Oguro H, Awaji S, Watanabe K, Sugano M, Machiya S, Shobu T, Sato M, Koganezawa T and Osamura K 2012 Internal strain measurement for Nb_3Sn wires using synchrotron radiation *Supercond. Sci. Technol.* **25** 054004

[9] Taylor D M J and Hampshire D P 2005 The scaling law for the strain dependence of the critical current density in Nb_3Sn superconducting wires *Supercond. Sci. Technol.* **18** S241–52

[10] Carty G J and Hampshire D P 2008 Visualising the mechanism that determines the critical current density in polycrystalline superconductors using time-dependent Ginzburg–Landau theory *Phys. Rev.* B **77** 172501

[11] Carty G J and Hampshire D P 2013 The critical current density of an SNS junction in high magnetic fields *Supercond. Sci. Technol.* **26** 065007

[12] Sunwong P, Higgins J S, Tsui Y, Raine M J and Hampshire D P 2013 The critical current density of grain boundary channels in polycrystalline HTS and LTS superconductors in magnetic fields *Supercond. Sci. Technol.* **26** 095006

[13] Muzzi L *et al* 2012 Direct observation of Nb_3Sn lattice deformation by high-energy x-ray diffraction in internal-tin wires subject to mechanical loads at 4.2 K *Supercond. Sci. Technol.* **25** 054006

[14] Osamura K, Machiya S, Tsuchiya Y and Suzuki H 2010 Internal strain and mechanical properties at low temperatures of surround Cu stabilized YBCO coated conductor *IEEE Trans. Appl. Supercond.* **20** 1532–6

[15] Kagiyama T *et al* 2011 Recent progress in high performance Ag-sheathed Bi2223 wire (DI-BSCCO®) *IOP Conf. Ser.: Mater. Sci. Eng.* **18** 152001

[16] Sunwong P, Higgins J S and Hampshire D P D P 2011 Angular, temperature and strain dependencies of the critical current of DI-BSCCO tapes in high magnetic fields *IEEE Trans. Appl. Supercond.* **21** 2840–4

[17] Osamura K, Machiya S, Suzuki H, Ochiai S, Adachi H, Ayai N, Hayashi K and Sato K 2009 Improvement of reversible strain limit for critical current of DI-BSCCO due to lamination technique *IEEE Trans. Appl. Supercond.* **19** 3026–9

[18] Sugano M, Shikimachi K, Hirano N and Nagaya S 2010 The reversible strain effect on critical current over a wide range of temperatures and magnetic fields for YBCO coated conductors *Supercond. Sci. Technol.* **23** 085013

[19] van der Laan D C, Haugan T J, Barnes P N, Abraimov D, Kametani F, Larbalestier D C and Rupich M W 2010 The effect of strain on grains and grain boundaries in $YBa_2Cu_3O_{7-\delta}$ coated conductors *Supercond. Sci. Technol.* **23** 014004

[20] Tanaka K, Suzuki K and Akiniwa Y 2006 *Evaluation of Residual Stresses by X-Ray Diffraction* (Tokyo: Yokendo Ltd)

[21] Clark S J 2013 University of Durham private communication